Available online at www.sciencedirect.com

ScienceDirect

Nuclear Physics A 967 (2017) 385–388

NUCLEAR PHYSICS A

www.elsevier.com/locate/nuclphysa

Anisotropic flow of inclusive and identified particles in Pb–Pb collisions at $\sqrt{s_{\mathrm{NN}}} = 5.02$ TeV with ALICE

R. A. Bertens (for the ALICE collaboration)

University of Knoxville (Tennessee USA), CERN

Abstract

Elliptic (v_2) and higher harmonic (v_3, v_4) flow coefficients of $\pi^{\pm}$, $K^{\pm}$, p($\overline{\mathrm{p}}$), and the ϕ-meson, measured in Pb-Pb collisions at the highest-ever center-of-mass energy of $\sqrt{s_{\mathrm{NN}}} = 5.02$ TeV, are presented. The results were obtained with the scalar product method, correlating hadrons with reference particles from a different η region. The v_n exhibit a clear mass ordering for $p_{\mathrm{T}} \lesssim 2$ GeV/c and only approximate particle type scaling for $p_{\mathrm{T}} \gtrsim 2$ GeV/c. Reasonable agreement with hydrodynamic calculations (IP-Glasma+MUSIC+UrQMD) is seen at $p_{\mathrm{T}} \lesssim 1$ GeV/c.

Keywords: anisotropic flow, heavy-ion, higher harmonic, identified, relativistic hydrodynamics

1. Introduction

Heavy-ion collision experiments are used to study the properties of the quark-gluon plasma (QGP), a state of deconfined quarks and gluons created at high baryon densities or temperatures. Particles produced in collisions are boosted collectively by a common velocity field that is induced by the rapid expansion of the system. Spatial anisotropies resulting from the elliptic overlap region of the colliding nuclei in non-central collisions, and the initial inhomogeneities of the system density, are transformed, through multiple interactions between the produced particles, into an anisotropy in momentum space of the produced particles. The efficiency of this process depends on e.g. the shear (η/s) and bulk (ζ/s) viscosity of the created matter, and the lifetime of the system.

Anisotropy in particle production can be quantified by a Fourier analysis of the azimuthal distribution relative to the system's symmetry plane angles Ψ_n, characterized by harmonic coefficients v_n [1]

$$\frac{\mathrm{d}N}{\mathrm{d}\left(\varphi - \Psi_n\right)} \propto 1 + \sum_{n=1}^{\infty} 2v_n \cos\left(n\left[\varphi - \Psi_n\right]\right), \tag{1}$$

where φ is the azimuthal angle of the produced particles.

Flow coefficients v_n are, in addition to being a probe for η/s and ζ/s, sensitive to the initial state of the system, freeze-out conditions and hadronization mechanisms.

Email address: redmer.alexander.bertens@cern.ch (R. A. Bertens (for the ALICE collaboration))

http://dx.doi.org/10.1016/j.nuclphysa.2017.04.025
0375-9474/

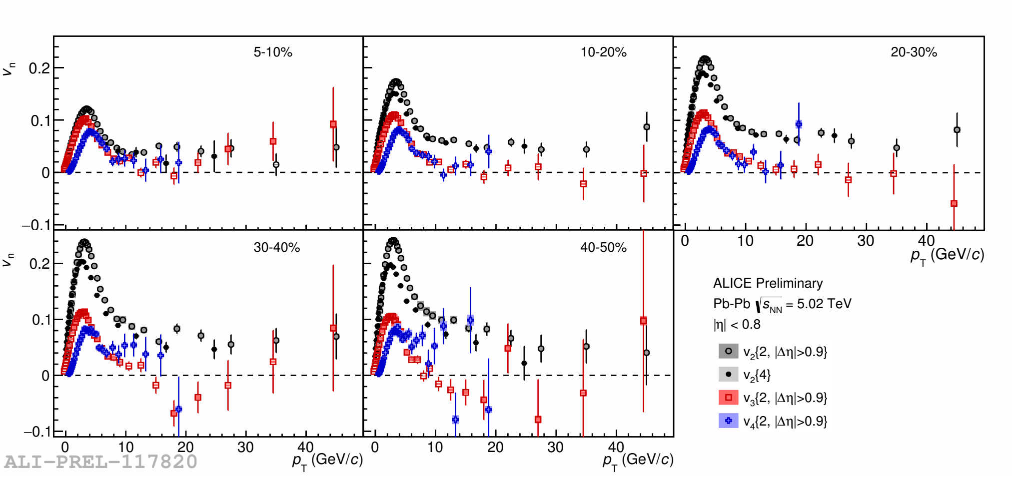

Fig. 1. Flow coefficients v_2, v_3 and v_4 of unidentified charged particles as function of p_T for various centrality classes. In addition to the scalar product method, the 4-particle Q-cumulant [5] estimate of v_2, $v_2\{4\}$, is shown as well. Statistical uncertainties are shown as bars and systematic uncertainties as boxes.

2. Data analysis

The data used for this work were recorded in 2015 at a center of mass energy per nucleon pair of $\sqrt{s_{NN}} =$ 5.02 TeV with the ALICE detector [2] and comprise approximately $6{\times}10^7$ collisions with a vertex within ±10 cm of the nominal interaction point and collision centrality between 5-60%. Charged particle tracks are reconstructed using the Inner Tracking System (ITS) and Time Projection Chamber (TPC) at $|y| < 0.5$ for identified particles or $|\eta| < 0.8$ for unidentified particles. Centrality determination, as well as reconstruction of the $\mathbf{Q}_n^{\mathrm{V0}}$ vectors (see Eq. 2), is performed with V0 detectors, located at $2.8 < \eta < 5.1$ (V0A) and $-3.7 < \eta < -1.7$ (V0C).

Coefficients v_n are measured using the scalar product method [3], written as

$$v_n\{\mathrm{SP, V0C}\} = \langle\langle \mathbf{u}_n \cdot \mathbf{Q}_n^{\mathrm{V0C}*}\rangle\rangle \Bigg/ \sqrt{\frac{\langle \mathbf{Q}_n^{\mathrm{V0C}} \cdot \mathbf{Q}_n^{\mathrm{TPC}*}\rangle\langle \mathbf{Q}_n^{\mathrm{V0C}} \cdot \mathbf{Q}_n^{\mathrm{V0A}*}\rangle}{\langle \mathbf{Q}_n^{\mathrm{TPC}} \cdot \mathbf{Q}_n^{\mathrm{V0A}*}\rangle}} \tag{2}$$

where $\mathbf{u}_n = \exp(in\varphi)$ is the unit vector of a single *particle of interest* (the particles of which v_n is measured), with azimuthal angle φ. Flow vectors $\mathbf{Q}_n = \sum_j \exp(in\varphi_j)$ of the *reference particles*, where the sum runs over all j tracks and * denotes the complex conjugate, are measured in the TPC or V0 detectors. Brackets $\langle \ldots \rangle$ indicate an all-event average; the double brackets in the numerator of Eq. 2 mean that prior to the all-event average, an average over all $\mathbf{u}_n \cdot \mathbf{Q}_n^{\mathrm{V0C}*}$ within the single event is taken. The large (pseudo-)rapidity gap between $\mathbf{u}_n$ and $\mathbf{Q}_n^{\mathrm{V0C}}$ reduces sensitivity to short-range correlations that are unrelated to the initial geometry, commonly referred to as *non-flow*.

Particle identification is performed using ionization energy loss measured in the TPC, combined with the arrival time of particles in the Time of Flight (TOF) detector. The ϕ-meson is reconstructed in the $\phi \to K^+K^-$ channel, using the analysis method outlined in [4].

3. Results

Figure 1 shows p_T-differential v_2, v_3 and v_4 of unidentified charged particles. For the presented centrality classes, $v_2 > v_3 > v_4$ for $p_T < 5$ GeV/c. The observed trends at low and intermediate p_T (< 7 GeV/c) are

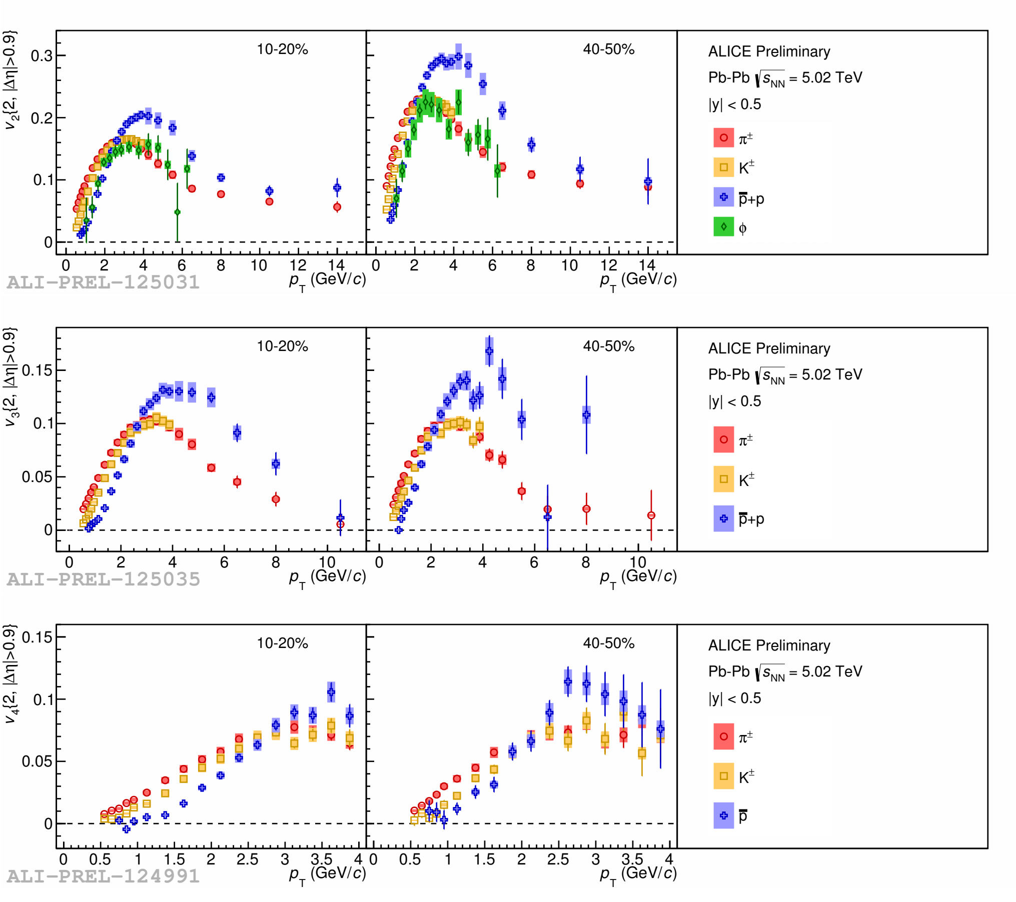

Fig. 2. Flow coefficient v_2 (top), v_3 (middle) and v_4 (bottom) of $\pi^{\pm}$, $K^{\pm}$, p($\overline{\text{p}}$) and the ϕ-meson for 10-20% (left) and 40-50% (right) collision centrality as function of p_T. Statistical uncertainties are shown as bars and systematic uncertainties as boxes.

characteristic for the hydrodynamic expansion of the medium. The non-zero v_2 at high p_T is attributed to path-length dependent in-medium energy loss of highly energetic partons.

The top panel of Fig. 2 shows p_T-differential v_2 of $\pi^{\pm}$, $K^{\pm}$, p($\overline{\text{p}}$) and the ϕ-meson for 10-20% (left) and 40-50% (right) collision centrality (these two centrality intervals are used for all subsequent figures; note that for $p_T < 4$ GeV/c only $\overline{\text{p}}$ are considered to exclude a contamination by secondary protons produced from detector material). For $p_T < 2$ GeV/c, v_2 of the different species is mass-ordered, which is indicative of strong radial flow [6]. For $3 < p_T < 8$ GeV/c, particles are grouped according to their valence quark content, which supports the hypothesis of particle production via quark coalescence [7]. Particle type scaling and mass ordering is most directly tested by ϕ-meson v_2, as the ϕ is a meson with a mass close to proton mass. Figure 2 demonstrates that ϕ-meson v_2 follows proton v_2 at low p_T, but pion v_2 at intermediate p_T. Lastly it should be noted that p($\overline{\text{p}}$) v_2 is larger than $\pi^{\pm}$ v_2 for $3 \lesssim p_T \lesssim 10$ GeV/c, after which the v_2 converge, which suggests that partonic energy loss is flavor independent at high transverse momenta.

Higher harmonic flow coefficients ($n > 2$) are generated by inhomogeneities in the initial nucleon distribution and are thought to be more sensitive to transport coefficients than v_2 [8]. The middle and lower panels of Fig. 2 show that non-zero v_3 is observed for $\pi^{\pm}$, $K^{\pm}$, p($\overline{\text{p}}$) up to $p_T \approx 8$ GeV/c. Statistical precision

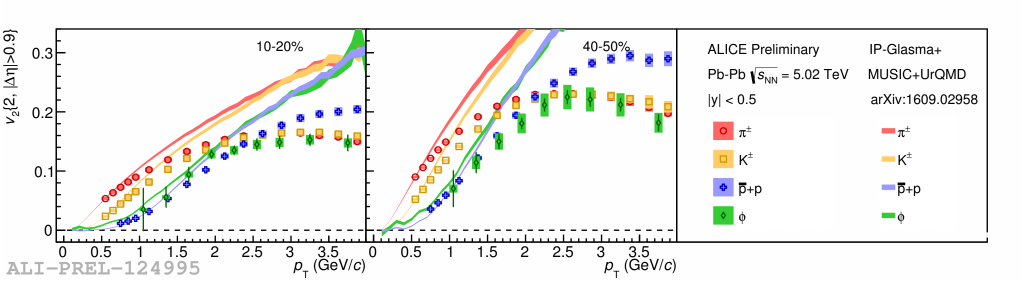

Fig. 3. Flow coefficient v_2 of $\pi^{\pm}, K^{\pm}$, p($\overline{\text{p}}$) and the ϕ-meson for 10-20% (left) and 40-50% (right) collision centrality compared to predictions from relativistic hydrodynamic calculations [10]. Statistical uncertainties are shown as bars and systematic uncertainties as boxes.

limits the range of the v_4 measurement to $p_T < 4$ GeV/c; v_4 is non-zero though in the entire measured range. Both v_3 and v_4 show a clear mass ordering at low p_T, and analogous to the trend of v_2, p($\overline{\text{p}}$) v_3 is larger than $\pi^{\pm}$ v_3 up to $p_T = 10$ GeV/c. The crossing of the meson and baryon trends at $p_T \approx 2.5$ GeV/c is reminiscent of the behavior observed for v_2 as well. Overall, the v_n values are qualitatively similar to those observed at a collision energy of $\sqrt{s_{NN}} = 2.76$ TeV [4, 9].

To test the validity of the hydrodynamic description of the QGP, v_n are compared to model predictions from [10] in Fig. 3. The model uses an IP-Glasma initial state and a viscous hydrodynamic medium evolution ($\eta/s = 0.095$ and a temperature-dependent ζ/s) which is coupled to a hadronic cascade procedure for hadronization. Interestingly, mass ordering is broken (ϕ-meson v_2 > p($\overline{\text{p}}$) v_2) in the calculations. The predictions show good agreement with the data for $p_T < 1$ GeV/c in central collisions, but overestimate v_2 already at lower p_T for more peripheral collisions. Similar behavior is found for v_3 and v_4 (not shown).

To test the hypothesis of particle production via quark coalescence, the axes of Fig. 2 can be scaled by the number of constituent quarks, independently for each species [7]. Such a scaling (not shown) shows that from $p_T/n_q > 1.5$ GeV/c particles group approximately according to their type (baryon, meson), similar behavior is observed for v_3 and v_4. It is stressed that the observed scaling only holds approximately, as was also observed elsewhere [4].

4. Summary

Flow harmonics v_2, v_3 and v_4 of unidentified and identified particles have been measured at $\sqrt{s_{NN}} = 5.02$ TeV Pb–Pb collisions. Mass ordering is observed for $p_T < 2$ GeV/c, as well as approximate particle type scaling for $p_T > 2.5$ GeV/c. The flow coefficient v_2 of unidentified particles is non-zero up to high p_T, and p($\overline{\text{p}}$) v_2 and v_3 are larger than $\pi^{\pm}$ v_2 and v_3 up to $p_T = 10$ GeV/c. The unprecedented precision of these new measurements will put strong constraints on model calculations and furthers the understanding of the hydrodynamic behavior of the QGP, as well as its initial state, and freeze-out conditions.

References

[1] J.-Y. Ollitrault, Phys. Rev. D46 (1992) 229–245.
[2] B. Abelev, et al., Int. J. Mod. Phys. A29 (2014) 1430044.
[3] S. A. Voloshin, A. M. Poskanzer, R. Snellings, arXiv:0809.2949.
[4] B. B. Abelev, et al., JHEP 06 (2015) 190.
[5] A. Bilandzic, R. Snellings, S. Voloshin, Phys. Rev. C83 (2011) 044913.
[6] P. Huovinen, P. F. Kolb, U. W. Heinz, P. V. Ruuskanen, S. A. Voloshin, Phys. Lett. B503 (2001) 58–64.
[7] D. Molnar, S. A. Voloshin, Phys.Rev.Lett. 91 (2003) 092301.
[8] G.-Y. Qin, H. Petersen, S. A. Bass, B. Muller, Phys. Rev. C82 (2010) 064903.
[9] K. Aamodt, et al., Phys. Rev. Lett. 107 (2011) 032301.
[10] S. McDonald, C. Shen, F. Fillion-Gourdeau, S. Jeon, C. Gale, arXiv:1609.02958.